Using pit solution chemistry for evaluation of metastable pitting stability of austenitic stainless steel

M. H. Moayed* and R. C. Newman

The stability of a corrosion pit is directly related to the pit solution chemistry. In order to know the stability of a meastable pit, the product of corrosion current density and diffusion depth (pit radius for an open hemisphere pit) is compared to the stability product obtained from the artificial pit electrode results. In this paper the stability of a metastable pit recorded on a 904L stainless at 54 °C (2 °C below the alloy CPT) is investigated. Assuming the geometry result of such a transient is an open hemisphere, pick current density and pit radius were calculated from Faraday's equation and then pit stability product (i·a) was calculated. This value was compared with the product of i·a associated with the pit solution chemistries (critical, saturation and supersaturation concentrations) which were obtained from the investigation on artificial pit electrode at the same temperature. SEM investigations on pit cavity generated from large metastable pit current transients with the stability product greater than the stability product associated with supersaturation concentration of pit environment proves that measured pit solution chemistry from artificial pit electrode is a reliable step for evaluation of pit stability.

1 Introduction

Several investigations have been carried out to find a criterion for stable pit growth. The result of all the works can be summarized as; the chemistry of the solution inside the pit which is concentrated in metal cations and chloride ions, somehow contribute to control pit stability. The dissolution kinetics within such a localized cell (pit cavity) would be expected to differ from that of a surface in direct contact with the bulk solution. *Pistorius* and *Burstein* [1] defined a critical value of the product of the pit radius and its dissolution current density (termed the pit stability product) for metastable to stable growth transition. Following the work of others [2] it was assumed that a minimum concentration of metal ions was necessary within the pit to maintain the required pH for active dissolution. Neglecting convection and migration, *Pistorius* and *Burstein* suggested that for an open, hemispherical pit of radius, a, the degree of concentration, ΔC, at the pit surface is given by:

$$\Delta C = \left(\frac{2\pi}{3nFD}\right)ia \qquad (1)$$

As established earlier by *Galvele* [3] the critical parameter is therefore the product of i·a, which *Pistorius* and *Burstein* [1] termed the stability product. For 304 SS, taking a minimum ΔC of 3 M and maximum of 6 M (allowing for supersaturation concentration), equation (2) was obtained showing the possible range of values of i·a for stable pit growth.

$$0.003 \ A \cdot cm^{-1} \le ia \le 0.006 \ A \cdot cm^{-1} \qquad (2)$$

They put forward that all pits, whether stable, or destined to become stable, grow initially in the metastable condition, with a pit stability product which increases linearly with time, but below the critical concentration value. Metastable growth requires a perforated cover over the pit mouth to provide an additional barrier to diffusion, enabling the aggressive pit anolyte to be maintained. Stable pit growth is then achieved when the cover is no longer required for continued propagation, and the pit depth is itself a sufficient diffusion barrier. If the cover is lost permanently, before the critical pit stability product is achieved, the pit anolyte is diluted and repassivation is inevitable [1, 4]. They also stated that all pits had salt films. *Sato* [5] proposed that for pit stability a critical concentration build-up ΔC^* of metal salt must be attained. The criterion determining the stability of pitting was given by; for stable pit growth $\Delta C > \Delta C^*$ and if for any reason the condition of $\Delta C < \Delta C^*$ is established, a growing pit is repassivated.

2 Experiment procedure

2.1 Electrochemical equipment

Throughout this work an ACM potentiostat (ACM instruments) was used to control the electrode potential. During the sweeping of the electrode potential, an ACM sweep generator (ACM instruments) was employed in connection with the potentiostat. The current between working and auxiliary electrodes was measured either by a digital electrometer in series with the cell or across a resistor inserted into the circuit. The analogue output of the electrometer or current output

* *M. H. Moayed*,
Metallurgical & Materials Engineering Department,
Faculty of Engineering, Ferdowsi University,
Mashhad, P.O. Box, 91775-1111 (Iran),
e-mail: mhmoayed@ferdowsi.um.ac.ir

R. C. Newman,
University of Toronto, Dept. of Chemical Engineering
and Applied Chemistry, 200 College Street, Toronto,
M5S 3E5, Ontario (Canada)

of the potentiostat was connected to an A/D card and the data were stored in a personal computer. In artificial pit electrode experiments the current was recorded directly by an A/D card connected to a PC and a chart recorder.

2.2 Potentiostatic measurement of critical pitting temperature

The potentiostatic CPT determination procedure involves polarization of the working electrode by applying a potential more noble than the pitting potential with continuously increasing temperature. The specimens were mounted into a cell containing 200 ml of 1 M NaCl with a temperature of less than 5 °C. In this work, all the specimens were allowed to stabilize at their open circuit potential for 5–10 min. at the starting temperature. After initial temperature stabilization, an anodic potential of 750 mV (vs. Ag/AgCl) was applied. For the CPT measurements on the plain electrodes, the electrode was polarized from the rest potential at a potential scan rate of 10 mV/s to 750 mV, to avoid the effect of sudden polarization and crevice corrosion. The cell current was recorded after 5 seconds from the beginning of each test. The electrolyte temperature was changed at a rate of ~ 0.4 °C/min. The CPT has been evaluated at which the current density exceeds from the base passive current without returning to the passive base current after one minute.

2.3 Potentiostatic measurement of metastable pit current transients

The main aim of these experiments was to calculate the anodic charge transfer of individual metastable pit transients at temperatures below the CPT. For this reason small working electrodes of ~ 0.1 cm^2 were used to record separated metastable pit events with no overlapping. The working electrode was held at its rest potential for 5 min. and then polarized with a scan rate of 10 mV/s to 750 mV. The current transients were recorded after 5 seconds from the beginning of the test at 750 mV. A 60 Hz data acquisition rate was used to minimize the error of calculation of anodic charge transferred due to each transient from the I-t curves.

2.4 Measuring of pit chemistry using artificial pit electrode

The artificial pit electrode measurements were carried out in a beaker of 250 ml open to air with a three-electrode system containing 1 M NaCl at several constant temperatures. After initial stabilization of the temperature at the open circuit potential, the specimen was polarized anodically by applying 750 mV. This potential is well above the pitting potential of 302 and 316 SS in 1 M NaCl. Formation and coalescence of salt covered pits leads to establishment of a steady state diffusion controlled regime. In diffusion controlled growth, the potential was stepped to 400 mV prior to backward scanning the potential. In order to measure the maximum supersaturation concentration of pit solution, the electrode potential was sometimes scanned forward from the activation/IR drop controlled regime. Throughout this work, potential scan rate of 4 mV/s was used. Pit solution chemistries including pit critical concentration (C*), pit saturation concentration (C$_s$), and pit supersaturation concentration (C$_{ss}$) were measured.

Table 1. Composition of the major alloying elements in the alloys used in this work

| Stainless Steel	Major Alloying Elements wt%				
Grade	Cr	Ni	Mo	N	Mn
302	19	11	–	–	< 2
316	20	11	2.54	–	< 2
904L	20	25	4.32	0.16	1.41

2.5 Pit morphology and qualitative analysis

Pit morphology was investigated using Scanning Electron Microscopy (SEM). SEM was operated using electrons with the accelerating potential 10 or 20 KV. Energy Dispersive X-ray Analysis (EDAX) technique was also employed for qualitative analysis of the passive film outside of pit cavity and polished interior pit surface areas. This method gives a reasonable qualitative elemental analysis for most elements simultaneously within few minutes. All materials used were austenitic stainless steel.

Three grades of stainless steel were used including 50 µm 302 and 316 wires supplied by Goodfellow and the highly alloyed 904L stainless steel by Avesta Polarit companies. The alloy compositions are given in Table 1.

3 Results and discussion

An example of the evaluation of critical pitting temperature by the potentiostatic method for 904L stainless steel is illustrated in Fig. 1 in which the final part of the current-temperature relation is shown. The CPT was evaluated as the temperature where stable pits start to grow. The results of four experiments are illustrated in Fig. 2. It is evident that the reproducibility of the results is in the range of 1 °C. According to equation (1), the pit stability product (i·a) of each pit may be calculated by knowing the product of D·ΔC, where D is diffusivity of metal cations and ΔC is the concentration difference of metal cations inside and outside the pit cavity. Assuming that the concentration of metal cations outside the pit
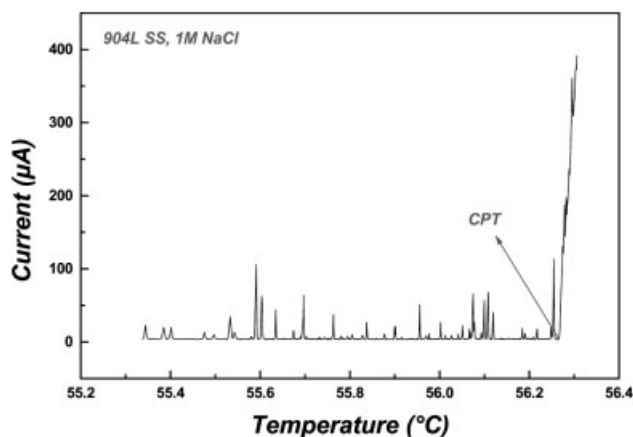
Fig. 1. Final part of current-temperature curves obtained from potentiostatic CPT measurements on 904L SS at 750 mV in 1 M NaCl solution
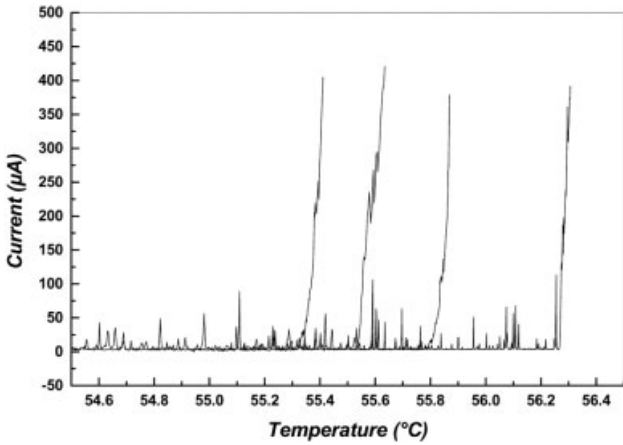
Fig. 2. Final part of four current-temperature curves obtained from potentiostatic CPT measurements on 904L SS at 750 mV in 1 M NaCl solution

is negligible, by knowing the concentration of metal cations inside the pit at the metal pit solution interface, the pit stability product can be calculated. In order to measure the values of D·ΔC several experiments were carried out on a 50 μm wire of 302 stainless steel at several temperatures. The experiments were carried out by applying an anodic potential of 750 mV on 50 μm 302 SS wire in 1 M NaCl, and measuring the limiting current density in the diffusion controlled regime as a function of time. Fig. 3 shows a typical plot of current density-time obtained from an artificial pit electrode experiment. Applying an anodic potential of 750 mV to a 50 μm 302 SS wire in 1 M NaCl, leads to unidirectional dissolution of the wire. In the first stage increasing of the current reveals formation of several stable pits. These pits are covered by a thin layer of metal/chloride salt. The second stage begins with a drop of current due to coalescence of pits and the total current now is limited by diffusion of metal cations from the metal/electrolyte interface to the bulk. In the second stage the current is potential independent and decreases as the pit depth increases. The length of the wire (h) dissolved during the course of the experiment is given by:

$$h = \frac{M_w}{nF\rho} \int idt \qquad (3)$$

where $\int idt$ is the surface area under the current density-time curve and M_w, n, F, and ρ are alloy molecular weight (55.38 gr/mole) [1], the valence of dissolved metal cations (2.19) [1], Faraday's constant (96485 C/mole) [1] and alloy density (7.92 gr/cm³) [6]. The variation of pit depth versus time for the current density-time curve in Fig. 3 is also illustrated at the same graph.

The ions produced in the oxidation reaction occurring at the metal surface will move through the solution under the influence of two forces, concentration gradients and potential gradients. It has been found that for 1 M NaCl and similar concentration solutions the potential gradient has less contribution to the total flux [7], so the obtained current is dominated by the diffusion gradient. By applying the first Fick's law, the current density in the diffusion controlled regime follows the following relation:

$$i_L = \frac{nFDC_s}{h} \qquad (4)$$

where C_s and h are the saturation concentration of metal cations and pit depth. Substituting Faraday's law, equation (3) into equation (4) and integration between $i_1 = 0$ at $t = 0$ and $i_2 = i$ at $t > 0$ yields:

$$i_L^2 = \frac{n^2F^2\rho DC_s}{2M_w t} \qquad (5)$$

Assuming that the values of n, F, ρ, and M_w are identical for 302 and 316 SS alloys, a plot of the square of pit limiting current density (i_L^2) as a function of the corresponding reciprocal of time (1/t) has a slope which is proportional to D·C_s. Fig. 4 shows the plot of the square pit current density at diffusion controlled regime versus reciprocal of time. It is evident that both alloys show the same slope and it may be concluded that the Mo content in the alloy 316 SS has no important contribution to the chemistry of the pit solution. This matter has been already mentioned by *Newman* [8, 9]. Therefore, doing experiments on artificial pit electrodes of 302 SS instead of highly alloyed 904L SS which contains more Mo, can be justified. In order to obtain pit chemistry, several artificial pit electrode experiments were carried out at different temperatures. Saturation concentration of pit electrolyte may be cal-
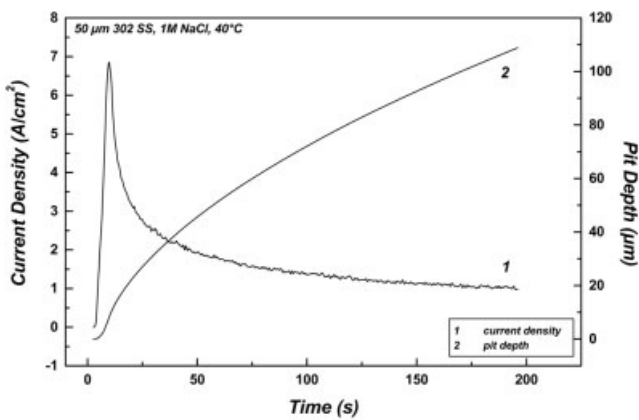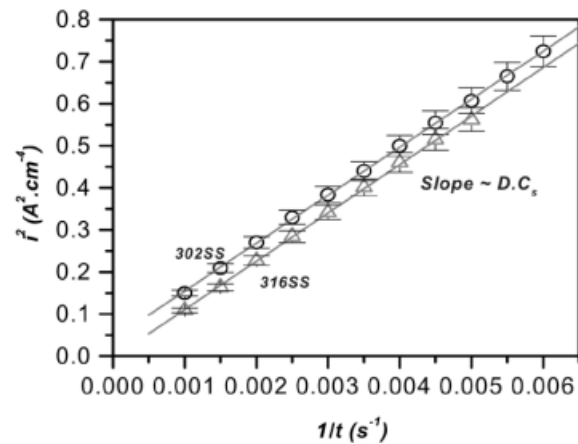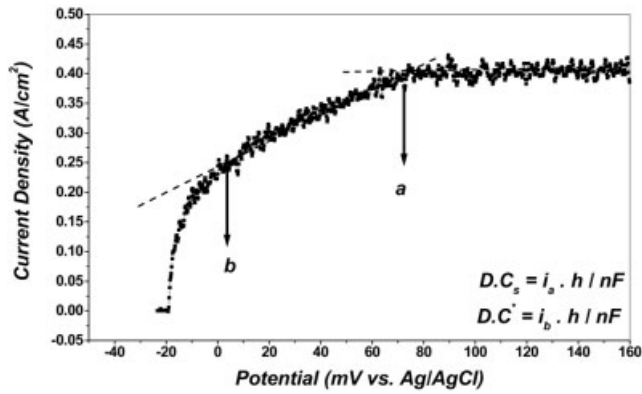

Fig. 3. Potentiostatic current time curve for 50 μm 302 SS wire at 750 mV in 1 M NaCl solution at 40 °C. Variation of pit depth with time was calculated from equation (3)

Fig. 4. Plot of i^2-1/t obtained from the current density-time curves using artificial pit electrodes of 50 μm 302 and 316 SS wire in 1 M NaCl solution at 750 mV at 40 °C

Fig. 5. Presentation of diffusion and activation/IR drop regimes using artificial pit electrode of 302 SS in 1 M NaCl solution at 40 °C. Activation/IR drop regime lies between point (a) and (b) where a linear relationship between current density and potential exists

Fig. 6. Presentation of diffusion and activation/IR drop regimes using artificial pit electrode of 302 SS in 1 M NaCl solution at 40 °C. The pit current increases at point (b) where the electrode potential was scanned forward

culated from the first Fick's law from the pit limiting current density in the diffusion controlled regime and knowing the pit depth (h):

$$D \cdot C_s = \frac{i_L h}{nF} \tag{6}$$

In the diffusion controlled regime the pit current is independent of the applied potential. Decreasing the current density is due to increasing of the pit depth (see equation (4)). In this stage the pit surface is covered with a thin layer of metal chloride salt, and the pit solution is saturated. The thickness of the salt film decreases as the potential decreases and it dissolves completely at the lower end of the diffusion controlled regime. From this stage (salt free) the current is potential dependent and any further decreasing of potential causes a decrease of current. Now the activation/IR drop controlled regime is established. The activation/IR drop controlled regime begins with a sharp deviation of limiting current density. This is indicated by point a in Fig. 5. The linear relationship between the current and potential in this stage reveals a potential dependence of current in the activation/IR drop controlled regime. The resistance of pit electrolyte may be defined from the slope of the potential-current relation in this stage. If the concentration profile remains linear throughout the pit depth, the ratio of the current corresponding to any point in the activation/IR-drop controlled regime to the current corresponding to the transition point (point a in Fig. 5) gives the salt concentration at the pit bottom as a fraction of saturation. The following relationship between the current and corresponding concentration may be written:

$$i_a = \frac{nFDC_s}{h} \tag{7}$$

$$i_b = \frac{nFDC}{h} \tag{8}$$

where C_s, and C are saturated concentration (mol/cm³) and the concentration of pit electrolyte at any stage in the activation\IR-drop controlled regime (mol/cm³). Since the pit depth is almost the same for point (*a*) and (*b*) (Fig. 5), and considering the same values for n, F, and D, the ratio of the currents at
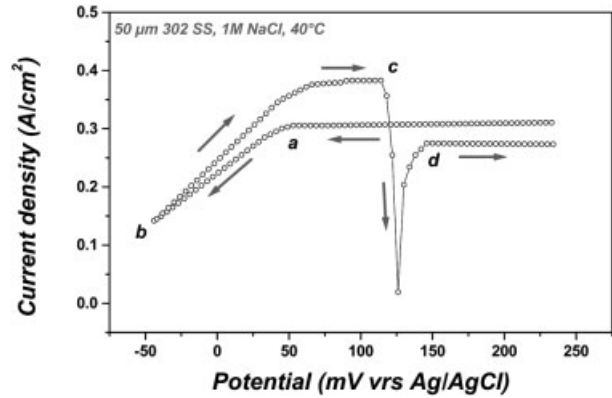
point (*b*) and (*a*) gives the fraction of pit saturation concentration:

$$\frac{i_b}{i_a} = \frac{C}{C_s} \tag{9}$$

If this fraction is less than a critical concentration (C*), forward scanning of the potential does not cause supersaturation of the pit solution but pit repassivation. It was found that forward scanning of the potential at any part of the activation\IR-drop controlled regime at which a linear relation between the current density and potential exists, allowed the pit solution to reach supersaturation concentration (point c in Fig. 6). Forward scanning of the potential at any point beyond this linearity (point k in Fig. 7) caused pit repassivation.

Since both the pit chemistry and metal cation diffusivity are affected by the temperature, in all calculations the values of D·C_s, and D·C* were considered. Pit critical concentration (C*) and saturation concentration (C_s) were calculated from the ratio of current densities corresponding to the point at the end of linearity of potential-current (point *b* in Fig. 5) and the transition between diffusion and activation\IR-drop controlled regimes (point *a* in Fig. 5):
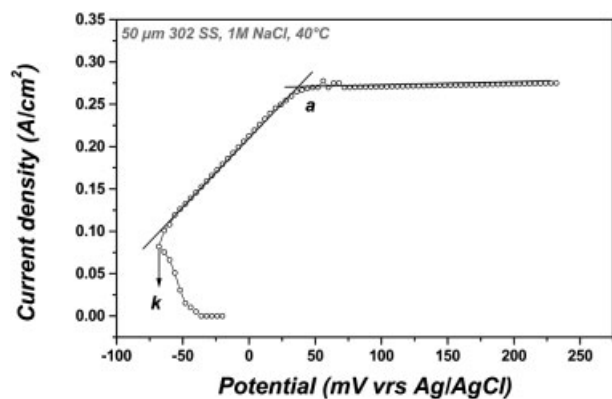

Fig. 7. Presentation of diffusion and activation/IR drop regimes using artificial pit electrode of 302 SS in 1 M NaCl solution at 40 °C. The pit is repassivated at point (k) when the electrode potential was scanned forward

$$D \cdot C_s = \frac{i_a h}{nF} \qquad (10)$$

$$D \cdot C^* = \frac{i_b h}{nF} \qquad (11)$$

where $D \cdot C^*$ and $D \cdot C_s$ have units of mol /cm.s. Forward scanning of the working electrode potential in the IR drop-activation regime leads to formation of a supersaturation concentration of pit solution (C_{ss}) (point c in Fig. 6) prior to re-establishment of the diffusion controlled regime (point d in Fig. 6). The following equation gives the necessary excess amount of metal cations in the pit to precipitate the new salt.

$$\frac{i_c}{i_d} = \frac{C_{ss}}{C_s} \qquad (12)$$

This ratio (C_{ss} / C_s) was found to be pit depth dependent and varied between 1.20 to 1.35. In this work the factor of 1.25 was used to calculate the value of C_{ss} from C_s ($D \cdot C_{ss} = 1.25 \times D \cdot C_s$).

Measurements of pit critical concentration $(D \cdot C^*)$ and pit saturation concentration $(D \cdot C_s)$ were carried out by running between 10–12 experiments at temperatures of 40, 45, 49, 54, 59 and 62 °C, at 750 mV in 1 M NaCl solution. In order to maintain linearity of pit concentration gradient at the activation/IR drop controlled regime, selecting the proper sweeping rate is important. In order to preserve the linear state of concentration profile in the pit, the duration of the activation/IR drop controlled regime should be greater than the time (τ) required for the metal cations to diffuse out of the pit with the depth of (h) which is given by the following equation:

$$\tau \cong \frac{h^2}{D} \qquad (13)$$

where D is the diffusivity of metal cations (cm^2/s). The potentiodynamic backscan rate carried out in this test was 4 mV/s. This rate was found sufficiently low in the case of pits with depth range of 100 to 150 µm to maintain a diffusional steady state when the current dropped below the limiting value and becomes activation/IR drop controlled. By considering a value of 1×10^{-5} (cm^2/s) for D, the values of τ were calculated for different pit depths according to the equation (13) and compared to the duration of the activation/IR drop controlled regime (the time between point a and b in Fig. 5), For a pit depth of 100–150 µm, τ was found to be 7–18 seconds

Table 2. A comparison between τ and the time to scan the potential range of activation/IR drop controlled regime at difference pit depths obtained from artificial pit electrode studies on 50 µm 302 SS wire in 1 M NaCl solution at 40 °C

Pit depth h (cm)	τ (s)	IR drop potential range (mV)	time to scan potential range (s)
0.0238	38	112	28
0.0202	27	100	25
0.0167	19	88	22
0.0136	12	74	18.5
0.0100	7	58	14.5

(Table 2). This time was lower than the duration (14.5-22 seconds) of the activation/IR drop controlled regime is lasted. Selection of a very low sweeping rate in backscanning of potential may cause a further growth of a pit in the activation/IR drop controlled regime and therefore i*/i$_L \neq$ C*/C$_s$. On the other hand for deeper pits (h > 200 µm), τ becomes greater than the duration of the activation/IR drop controlled regime. The maintenance of a diffusional steady state in this case may be slightly affected by the "fast" scan rate, and a lower scan rate should have been used to maintain a diffusional steady state.

Tables 3–5 show an example of the results of $D \cdot C_s$ and $D \cdot C^*$ values obtained for three temperature of 40, 49 and

Table 3. Values of $D \cdot C_s$ and $D \cdot C^*$ calculated from artificial pit electrode studies on 50 µm 302 SS in 1 M NaCl solution at 40 °C. Potential scan rate is 4 mV/s

Pit depth (µm)	$D \cdot C^*$ (mol/cm.s)	$D \cdot C_s$ (mol/cm.s)
134	3.504×10^{-8}	5.733×10^{-8}
94	3.342×10^{-8}	5.792×10^{-8}
97	3.710×10^{-8}	6.029×10^{-8}
110	3.783×10^{-8}	6.000×10^{-8}
127	3.912×10^{-8}	$6-018 \times 10^{-8}$
132	3.435×10^{-8}	5.309×10^{-8}
149	3.526×10^{-8}	5.642×10^{-8}
Average	3.614×10^{-8}	5.814×10^{-8}

Table 4. Values of $D \cdot C_s$ and $D \cdot C^*$ calculated from artificial pit electrode studies on 50 µm 302 SS in 1 M NaCl solution at 49 °C. Potential scan rate is 4 mV/s
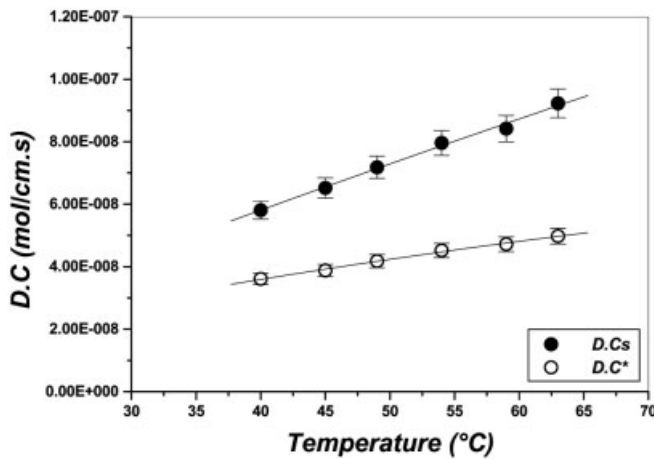
Pit depth (µm)	$D \cdot C^*$ (mol/cm.s)	$D \cdot C_s$ (mol/cm.s)
103	4.051×10^{-8}	6.382×10^{-8}
101	4.639×10^{-8}	7.137×10^{-8}
137	4.368×10^{-8}	7.313×10^{-8}
148	3.865×10^{-8}	7.729×10^{-8}
141	4.175×10^{-8}	7.015×10^{-8}
120	4.389×10^{-8}	7.702×10^{-8}
114	3.768×10^{-8}	6.998×10^{-8}
Average	4.180×10^{-8}	7.183×10^{-8}

Table 5. Values of $D \cdot C_s$ and $D \cdot C^*$ calculated from artificial pit electrode studies on 50 µm 302 SS in 1 M NaCl solution at 59 °C. Potential scan rate is 4 mV/s

Pit depth (µm)	$D \cdot C^*$ (mol/cm.s)	$D \cdot C_s$ (mol/cm.s)
98	4.872×10^{-8}	8.120×10^{-8}
104	4.671×10^{-8}	8.113×10^{-8}
131	4.808×10^{-8}	8.685×10^{-8}
141	4.842×10^{-8}	8.683×10^{-8}
149	4.280×10^{-8}	8.560×10^{-8}
113	4.837×10^{-8}	8.331×10^{-8}
Average	4.719×10^{-8}	8.416×10^{-8}

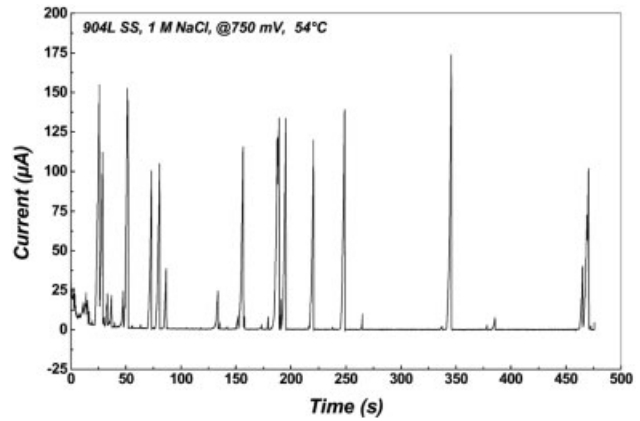**Table 6.** Average values of D·C$_s$ and D·C* at different temperatures

Temperature (°C)	D · C* (mol/cm.s)	D · C$_s$ (mol/cm.s)
40	3.614×10^{-8}	5.814×10^{-8}
45	3.877×10^{-8}	6.523×10^{-8}
49	4.180×10^{-8}	7.183×10^{-8}
54	4.520×10^{-8}	7.956×10^{-8}
59	4.719×10^{-8}	8.416×10^{-8}
62	4.980×10^{-8}	9.233×10^{-8}

Fig. 9. Current transients from metastable pit growth for electrode of type 904L stainless steel anodically polarized at 750 mV in a solution of 1 M NaCl at 54 °C

Fig. 8. Plot of average values of D·C$_s$ and D·C* at different temperatures using 50 μm wire of 302 SS in 1 M NaCl solution. Error bars show 95% confidence band

59 °C from the artificial pit electrode studies on 302 SS in 1 M NaCl solution with the backscanning potential scan rate of 4 mV/s. These results cover the pits with final depth between 100 and 150 μm. The average values of measurements were used in the calculation of pit stability products (Table 6). Fig. 8 illustrates the average values of pit chemistry as a function of temperature. It is shown that D·C$_s$ increases more than D·C* with the increase of temperature.

As mentioned earlier, concentration build-up in the pit electrolyte for an open hemispherical pit, growing under the diffusion controlled regime, is proportional to the product of pit current density (i) and pit radius (a) according to the equation

(1). Considering n = 2.19 and F = 96485 C/mol, the equation yields:

$$D \cdot \Delta C = 9.912 \times 10^{-6} \cdot (i \cdot a) \qquad (14)$$

where D and ΔC are diffusivity of metal cations and difference in concentration of metal cation inside and outside of the pit ($\Delta C = C - C_b$). Since $C_b \cong 0$, in 1 M NaCl solution therefore:

$$D \cdot C = 9.912 \times 10^{-6} \cdot (i \cdot a) \qquad (15)$$

The concentration build-up inside the pit (C) may be varied between the pit critical concentration (C*) to pit supersaturation concentration (C$_{ss}$). The values of pit stability product can be calculated for different pit chemistries for various temperatures as follows:

$$i \cdot a = 100888 \cdot (DC) \qquad (16)$$

i·a was calculated for different pit chemistries (e.g., D·C*, D·C$_s$, and D·C$_{ss}$) and the results are presented in Table 7. These data obtained from artificial pit electrode were used to know the stability products of metastable pits at temperature below the CPT.

Fig. 9 illustrates the result of current-time behavior of potentiostatic experiment on 904L SS at applied 750 mV anodic potential at 54 °C which is just ∼2 °C below the alloy CPT. Fig. 10 displays the characteristic shape of a metastable pit-

Table 7. Values of pit stability product (i·a) of different pit solution concentrations employing equation (1) for different temperatures, using 50 μm artificial pit electrodes of 302 SS in 1 M NaCl

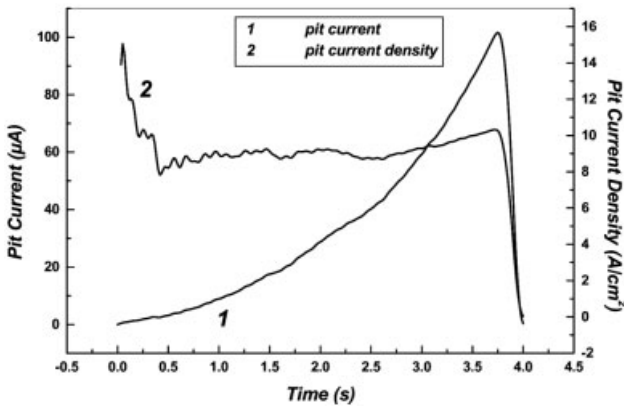| Temperature (°C) | Stability Product \ i·a (A/cm) | | |
	Critical Conc.	Saturation Conc.	Supersaturation Conc.
40	0.003646	0.005866	0.007332
45	0.003911	0.006581	0.008226
49	0.004217	0.007247	0.009058
54	0.004560	0.008027	0.010033
59	0.004761	0.008892	0.011115
62	0.005024	0.009315	0.011644

Fig. 10. Metastable pit current and current density plots of 904L SS at 750 mV in 1 M NaCl solution at 54 °C
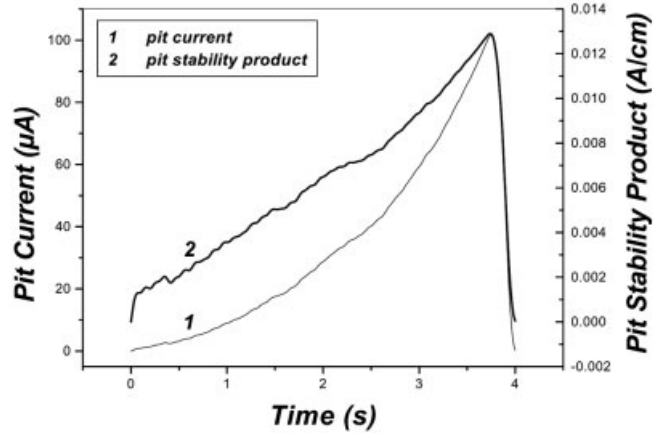

Fig. 12. Metastable pit current and stability product plot of 904L SS at 750 mV in 1 M NaCl solution at 54 °C

ting transient from Fig. 9. Integration of the current-time record from each transient gives the anodic charge that passed during growth. The radius of each pit was calculated from the anodic charge by using Faraday's law on the assumptions that the pit was hemispherical and the metallic components of the alloy are oxidized to Fe^{2+}, Cr^{3+} during dissolution. From Faraday's law, a relationship between the weight of the alloy per unit anodic charge (Q) due to dissolution of the alloy by knowing the valence of alloy dissolution (n), alloy density (ρ) and its molecular weight (M_w) can be established. The volume (V) of metal dissolved per unit anodic charge, K_v, may be calculated:

$$K_V = \frac{V}{Q} = \frac{M_w}{nF\rho} \tag{17}$$

By considering values of 55.79 g/mol, 2.19, 96485 C/mol and 7.97 g/cm^3 for M_w, n, F, and ρ, the value of 3.312×10^{-5} cm^3/C is obtained. The values of n and F were considered the same for 302, 316 and 904L stainless steels, but M_w and ρ values were calculated for 904L SS, knowing its composition and considering Fe^{2+} and Cr^{3+} are the main cations produced during the dissolution of the alloy. The anodic charge, Q (A·s), of each transient was calculated from the current-time relationship and then the radius, a (cm), and current density (A/cm^2) corresponding to the peak current of each transient
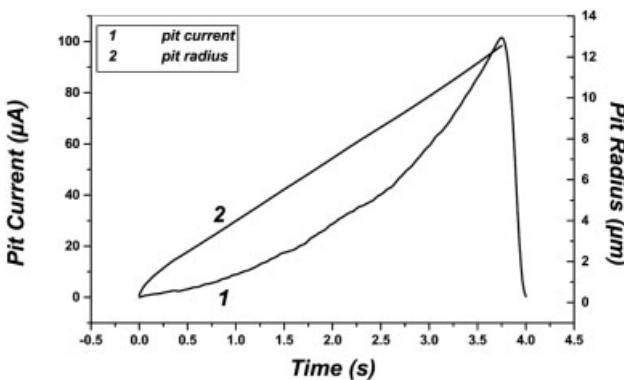
were calculated. The pit stability product, i·a (A/cm), was obtained from the product of the pit current density and radius. In order to calculate the anodic charge transferred from each transient, the passive current was subtracted from the original plot and each individual transient was isolated to give the current versus time plot. Figs. 11–13 illustrate the current density-time, pit radius-time and pit stability product-time variation for current-time behavior in Fig. 10. Three horizontal lines in Fig. 13 indicate the stability product corresponding with the pit critical, saturation and supersaturation concentrations obtained from artificial pit electrode experiments. It is evident that pit solution concentration of this pit has reached beyond to a value for precipitation of a salt layer. Therefore the morphology of such a pit is a polished interior surface. Fig. 14 shows EM pictures of such a metastable pit. From polished pit surface, it is clear that the pit has been grown under the metal chloride salt layer for some time and then repassivated. It means that precipitation of the salt layer inside the pit
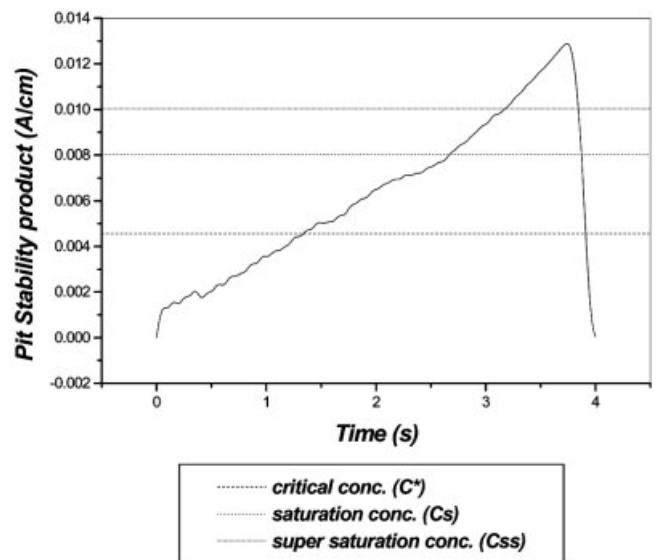

Fig. 13. Variation of pit stability product with metastable pit lifetime of 904L SS at 750 mV in 1 M NaCl solution at 54 °C. Three horizontal lines show the stability product associated with C*, C_s and C_{ss} obtained from artificial pit electrode studies according to formula (16)

Fig. 11. Calculated radius transient derived from metastable pit current transient of 904L SS at 750 mV in 1 M NaCl solution at 54 °C
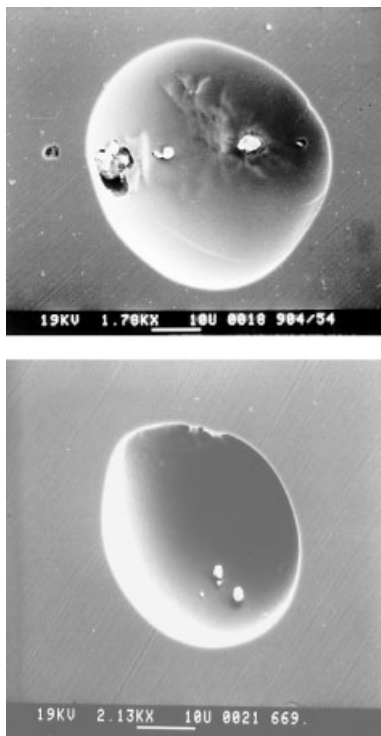
Fig. 14. SEM photomicrographs of polished metastable pit on a 904L SS sample after potentiostatic test at 750 mV in 1 M NaCl solution at 54 °C. This open hemisphere polished pit resulted from large metstable pit current transients with pick stability product greater than the stability product associated with supersaturation concentration
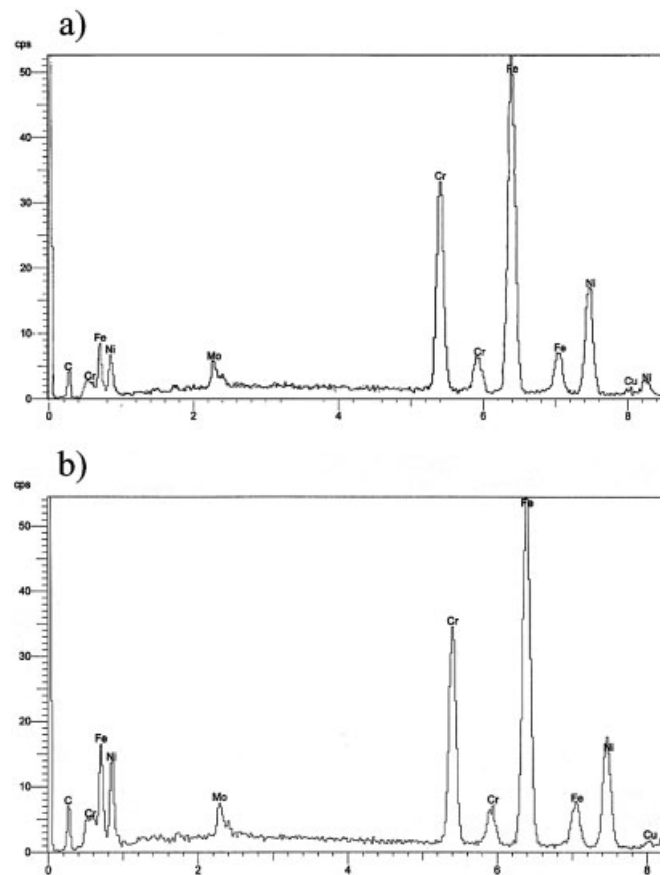
Fig. 15. EDAX analysis of passive area outside (a) and inside (b) the pit cavity similar to those illustrated in Fig. 14

cavity does not prepare all necessary conditions for stability of a metastable pit. In our studies [10–14] we have shown that although precipitation of a metal chloride salt layer in the pit cavity is a necessary criteria for pit stability but at the same time formation of a lacy cover over the pit mouth gives all criteria for pit stability. EDAX analysis (Fig. 15) of the passive area outside the pit and the interior surface of the polished pit reveals almost the same qualitative analysis. This means that after repassivation of the corrosion pit, a passive layer similar to the passive film outside the pit covers the pit surface.

4 References

[1] P. C. Pistorius, G. T. Burstein, *Philosophical Transaction Royal Society of London Academy* **1992**, *341*, 531.
[2] N. Sato, *Journal of Electrochemical Society* **1982**, *129*, 260.
[3] J. R. Galvele, *Journal of Electrochemical Society* **1976**, *123*, 464.
[4] D. E. Williams, R. C. Newman, Q. Sang, R. G. Kelly, *Nature* **1991**, *350*, 216.
[5] N. Sato, *Corrosion Science* **1995**, *47*, 1947.
[6] *G. C. limited, Goodfellow Cataluge*, Cambridge, CB4 4DJ, England, 333, **1999**.
[7] H. S. Isaacs, *Journal of Electrochemical Society* **1975**, *120*, 1438.
[8] R. C. Newman, *Corrosion Science* **1985**, *25*, 331.
[9] R. C. Newman, *Corrosion Science* **1985**, *25*, 341.
[10] P. Ernst, N. J. Laycock, M. H. Moayed, R. C. Newman, *Corrosion Science* **1997**, *29*, 1133.
[11] P. Ernst, M. H. Moayed, R. C. Newman, in: *Pits and Pores: Significance for Advanced Luminescent Materials*, ed. D. J. Leckwood and P. Schmuki, The Electrochemical Society, **1997**.
[12] P. Ernst, M. H. Moayed, N. J. Leycock, R. C. Newman, in: *Proceedings of Passivity of Metals and Semiconductors*, Jasper, Canada **1999**.
[13] N. J. Laycock, M. H. Moayed, R. C. Newman, *Journal of Electrochemical Society* **1998**, *145*, 2622.
[14] N. J. Laycock, S. P. White, J. S. Noh, P. T. Wilson, R. C. Newman, *Journal of Electrochemical Society*, **1998**, *145*, 1101.